Proceedings of the 2003 IEEE/RSJ
Intl. Conference on Intelligent Robots and Systems
Las Vegas, Nevada · October 2003

Recognizing Cylindrical Surface Using Impedance Perception

Ryo Kikuuwe
Department of Mechanical Engineering
Nagoya Institute of Technology
Nagoya 466-8555, Japan
kikuuwe@ieee.org

Tsuneo Yoshikawa
Department of Mechanical Engineering
Kyoto University
Kyoto 606-8501, Japan
yoshi@mech.kyoto-u.ac.jp

***Abstract*— In a previous paper, we proposed the impedance perception technique, by which the stiffness matrix that constrains the motion-force relation of the robot's end-effector is estimated on-line, and the uncertainties of the estimates are evaluated. Based on this technique, this paper proposes a method of extracting information on local properties of a cylindrical curved surface, including normal direction, primary directions, curvature, and stiffness and friction coefficients, from the stiffness matrix obtained under the situation where the end-effector is slid on the surface. This technique can be implemented as an encapsulated perception function independent from control strategies, and thus it can be used for both autonomous and remote-controlled robots, and for direct monitoring of human manipulations. Results of preliminary experiments are presented.**

I. Introduction

Recognizing shapes and properties of environments and objects are dispensable ability for adaptive robots. When the robot is directly in contact with the environment, the sensor data of position and force are important to perceive dynamic and local properties of the environment. Comparing to active probing strategies[1], passive monitoring of the sensor data without using any specialized control methods[2, 3] is less efficient but allows for easy implementation. Hence it has a potential to be used not only for autonomous robots but also for manually controlled robots and, moreover, for direct monitoring of human manipulations[4]. Researches on this kind of schemes are limited to non-deformable environments by using geometric constraint among objects. Tactile sensors can be used for the same purpose[5, 6], but those still need improvement in some aspects, and can not easily deal with the situation where the robot indirectly interacts with the environment through a tool.

The authors proposed the impedance perception technique in a previous paper[7], which is for identifying constraint conditions based on passive monitoring of position and force sensor data. Using this method, mechanical impedance parameters that constrain the motion of the robot's end-effector are estimated on-line in all directions at one time, and the uncertainties of the estimates are evaluated. Subsequently, the authors proposed a method to estimate the normal direction and the stiffness and friction coefficients of a flat surface, based on the stiffness matrix provided by the impedance perception, under the situation where the end-effector is slid on the surface[8]. Further enhancement has been required for this method since it cannot deal with curved surfaces. As an early effort in this direction, this paper proposes a new method to deal with cylindrical surfaces. In this method, the normal and primary directions, curvature, stiffness coefficient, and friction coefficient are estimated. Our everyday circumstances include many cylindrical objects such as pipes, bottles, and cans. Hence it is important to recognize information on this kind of objects by random and brief contacts, especially in order to instantaneously decide grasping strategies. For this method, the only required condition is a kinetic friction state on the surface, thus no autonomous action-generating function is required, and easy implementation for a broad range of application is expected.

In the rest of this paper, section II gives a brief review on the method to obtain a stiffness matrix using the impedance perception. Section III proposes the new method for estimating the properties of a cylindrical surface. Section IV presents the experimental results. Conclusion is provided in section V.

II. Stiffness Matrix Provided by the Impedance Perception

In the impedance perception technique [7], the position of the robot's end-effector, $\boldsymbol{p}(t) \in \mathcal{R}^3$, and the force applied to the end-effector from the environment, $\boldsymbol{f}(t) \in \mathcal{R}^3$, are fitted to a linear dynamic equation. The recursive least squares method with forgetting factor is employed for estimating the coefficients. The uncertainties of the estimates are determined based on the residual fitting error and distribution of the explanatory vectors, i.e., $\boldsymbol{p}(t)$, $\dot{\boldsymbol{p}}(t)$, and $\ddot{\boldsymbol{p}}(t)$.

The fitting equation is given as follows;

$$\boldsymbol{f}(t) = \boldsymbol{c} + \boldsymbol{K}\boldsymbol{p}(t) + \boldsymbol{B}\dot{\boldsymbol{p}}(t) + \boldsymbol{M}\ddot{\boldsymbol{p}}(t), \qquad (1)$$

where $\boldsymbol{K}, \boldsymbol{B}$ and $\boldsymbol{M} \in \mathcal{R}^{3\times3}$ are the matrices of stiffness, viscosity and inertia respectively that the robot perceives. Those matrices are dependent on the dynamic properties of the end-effector and the environment, and the contact configuration between them. $\boldsymbol{c} \in \mathcal{R}^3$ is a constant vector which corresponds to the equilibrium point of the stiffness, a force bias resulting from the gravitation, and etc.

Using Laplace transform and the bilinear transform, (1)'s discrete-time approximation is written as follows;

$$\boldsymbol{\phi}_k = \boldsymbol{\Theta}^T \boldsymbol{\psi}_k \quad (2)$$

$$\boldsymbol{\phi}_k \triangleq \boldsymbol{f}_k + 2\boldsymbol{f}_{k-1} + \boldsymbol{f}_{k-2} \quad \in \mathcal{R}^3 \quad (3)$$

$$\boldsymbol{\psi}_k \triangleq \left[\begin{array}{cccc} 1 & \boldsymbol{p}_k{}^T & \boldsymbol{p}_{k-1}{}^T & \boldsymbol{p}_{k-2}{}^T \end{array}\right]^T \quad \in \mathcal{R}^{10} \quad (4)$$

$$\boldsymbol{\Theta} \triangleq \left[\begin{array}{c} 4\boldsymbol{c}^T \\ \boldsymbol{K}^T + 2\boldsymbol{B}^T/T + 4\boldsymbol{M}^T/T^2 \\ 2\boldsymbol{K}^T - 8\boldsymbol{M}^T/T^2 \\ \boldsymbol{K}^T - 2\boldsymbol{B}^T/T + 4\boldsymbol{M}^T/T^2 \end{array}\right] \in \mathcal{R}^{10\times 3}, \quad (5)$$

where T is the sampling period and the subscript k denotes the value of the variable at time instant kT.

At time instant kT, the weighted sum-of-products matrix of the residual fitting errors is written as;

$$\begin{aligned} \boldsymbol{J}_k(\boldsymbol{\Theta}) &\triangleq \sum_{i=i_0}^{k} w_{k,i}(\boldsymbol{\phi}_i - \boldsymbol{\Theta}^T\boldsymbol{\psi}_i)(\boldsymbol{\phi}_i - \boldsymbol{\Theta}^T\boldsymbol{\psi}_i)^T \\ &= \boldsymbol{\Theta}^T\boldsymbol{R}_k\boldsymbol{\Theta} - \boldsymbol{Q}_k{}^T\boldsymbol{\Theta} - \boldsymbol{\Theta}^T\boldsymbol{Q}_k + \boldsymbol{F}_k \ , \quad (6) \end{aligned}$$

where $\{w_{k,i}\}_{i_0\le i\le k}$ denotes the weighting sequence at time instant kT, i_0 is the time instant at which the calculation starts, $\boldsymbol{R}_k \triangleq \sum_{i=i_0}^{k} w_{k,i}\boldsymbol{\psi}_i\boldsymbol{\psi}_i{}^T$, $\boldsymbol{Q}_k \triangleq \sum_{i=i_0}^{k} w_{k,i}\boldsymbol{\psi}_i\boldsymbol{\phi}_i{}^T$, and $\boldsymbol{F}_k \triangleq \sum_{i=i_0}^{k} w_{k,i}\boldsymbol{\phi}_i\boldsymbol{\phi}_i{}^T$. The weighting is designed dependent on the speed of the movement, so that the estimate is updated more rapidly during high-speed motion of the end-effector.

When $\boldsymbol{R}_k{}^{-1}$ exists, (6) is transformed as follows;

$$\boldsymbol{J}_k(\boldsymbol{\Theta}) = (\boldsymbol{\Theta}-\hat{\boldsymbol{\Theta}}_k)^T\boldsymbol{R}_k(\boldsymbol{\Theta}-\hat{\boldsymbol{\Theta}}_k)+\boldsymbol{S}_k \quad (7)$$

$$\hat{\boldsymbol{\Theta}}_k \triangleq \boldsymbol{R}_k{}^{-1}\boldsymbol{Q}_k \ \in \mathcal{R}^{10\times 3} \quad (8)$$

$$\boldsymbol{S}_k \triangleq \boldsymbol{F}_k - \boldsymbol{Q}_k{}^T\boldsymbol{R}_k{}^{-1}\boldsymbol{Q}_k \ \in \mathcal{R}^{3\times 3}. \quad (9)$$

Since $\boldsymbol{R}_k$ is positive definite, $\boldsymbol{J}_k(\boldsymbol{\Theta}) \succeq \boldsymbol{J}_k(\hat{\boldsymbol{\Theta}}_k) = \boldsymbol{S}_k$ is satisfied for any $\boldsymbol{\Theta}$ ($\boldsymbol{X} \succeq \boldsymbol{Y}$ means that $\boldsymbol{X}-\boldsymbol{Y}$ is positive semi-definite). Therefore, $\hat{\boldsymbol{\Theta}}_k$ is adopted as the estimate of $\boldsymbol{\Theta}$ at time instant kT

Since $\boldsymbol{J}_k(\boldsymbol{\Theta}) \succeq \boldsymbol{S}_k$, $\boldsymbol{S}_k$ is the minimum of $\boldsymbol{J}_k(\boldsymbol{\Theta})$ in the partial order relation "$\preceq$". Normalizing $\boldsymbol{J}_k(\boldsymbol{\Theta})$ with respect to its minimum $\boldsymbol{S}_k$, a generalized distance measure from $\hat{\boldsymbol{\Theta}}_k$ to a given $\boldsymbol{\Theta}$ can be defined by

$$\begin{aligned} D_{\Theta,k}(\boldsymbol{\Theta}) &= \mathrm{tr}\left(\boldsymbol{S}_k^{-\frac{1}{2}}\left(\boldsymbol{J}_k(\boldsymbol{\Theta}) - \boldsymbol{S}_k\right)\boldsymbol{S}_k^{-\frac{1}{2}}\right) \\ &= \mathrm{cs}[\boldsymbol{\Theta} - \hat{\boldsymbol{\Theta}}_k]^T\left(\boldsymbol{S}_k{}^{-1}\otimes\boldsymbol{R}_k\right)\mathrm{cs}[\boldsymbol{\Theta} - \hat{\boldsymbol{\Theta}}_k], \end{aligned}$$

where $\otimes$ denotes the Kronecker Product operator and $\mathrm{cs}[\ \cdot\ ]$ denotes the vectorization operator that stacks the columns of the argument matrix. The uncertainty ellipsoid of $\hat{\boldsymbol{\Theta}}_k$ can be defined as a set of $\boldsymbol{\Theta}$'s which satisfy $D_{\Theta,k}(\boldsymbol{\Theta}) < 1$.

If $\boldsymbol{p}(t)$ in (1) is substituted by the true position measured by the sensors, the estimated impedance can become very unstable in rigid (or nearly rigid) contact situations. This problem is avoided by implementing a computer-simulated virutal soft cover around the real end-effector. The displacement of the *virtual soft finger*(hereinafter, VSF), $\Delta\boldsymbol{p}_{\mathrm{v}}(t)$, is simulated by solving the dynamic equation $\boldsymbol{f}(t) = K_{\mathrm{v}}\Delta\boldsymbol{p}_{\mathrm{v}}(t) + B_{\mathrm{v}}\Delta\dot{\boldsymbol{p}}_{\mathrm{v}}(t)$, where K_{v} and B_{v} are design parameters which represent the stiffness and viscosity coefficients of the VSF, and $\boldsymbol{f}(t)$ is the force observed by the sensor. The position of the VSF is determined by $\boldsymbol{p}(t) = \boldsymbol{p}_{\mathrm{r}}(t)+\Delta\boldsymbol{p}_{\mathrm{v}}(t)$, where $\boldsymbol{p}_{\mathrm{r}}(t)$ denotes the real position observed by the sensors. Substituting $\boldsymbol{p}(t)$ in (1) with the virtual position, the estimates are stabilized even in rigid contact states. The impedance estimated through the VSF is that of the serial-coupled system of the VSF and the real environment. In passive environments, the theoretical upper bound of stiffness coefficients estimated through the VSF is K_{v}.

According to the relation (5), the estimate of the stiffness matrix $\boldsymbol{K}$ is obtained by $\hat{\boldsymbol{K}}_k \triangleq \hat{\boldsymbol{\Theta}}_k{}^T\boldsymbol{T}$ where $\boldsymbol{T}$ ($\in \mathcal{R}^{10\times 3}$) is a certain constant matrix. Multiplying

$$\mathrm{vec}\left[(\boldsymbol{\Theta} - \hat{\boldsymbol{\Theta}}_k)^T\right]\mathrm{vec}\left[(\boldsymbol{\Theta} - \hat{\boldsymbol{\Theta}}_k)^T\right]^T \preceq \boldsymbol{R}_k^{-1}\otimes\boldsymbol{S}_k,$$

which is equivalent to $D_{\Theta,k}(\boldsymbol{\Theta}) < 1$, by $\boldsymbol{I}_3\otimes\boldsymbol{T}$ from the right and $\boldsymbol{I}_3\otimes\boldsymbol{T}^T$ from the left yields

$$\mathrm{vec}\left[\boldsymbol{K}-\hat{\boldsymbol{K}}_k\right]\mathrm{vec}\left[\boldsymbol{K}-\hat{\boldsymbol{K}}_k\right]^T \preceq \boldsymbol{\Pi}_k, \quad (10)$$

where $\boldsymbol{\Pi}_k \triangleq \boldsymbol{P}_k\otimes\boldsymbol{S}_k$, $\boldsymbol{P}_k \triangleq \boldsymbol{T}^T\boldsymbol{R}_k{}^{-1}\boldsymbol{T}$, and $\boldsymbol{I}_3$ stands for a 3×3 identity matrix. This represents the uncertainty ellipsoid of $\hat{\boldsymbol{K}}_k$, and is denoted as $\hat{\boldsymbol{\mathcal{E}}}_k$. A generalized distance from $\hat{\boldsymbol{K}}_k$ to a given $\boldsymbol{K}$ can be defined by

$$D_k(\boldsymbol{K}) \triangleq \mathrm{vec}\left[\boldsymbol{K}-\hat{\boldsymbol{K}}_k\right]^T\boldsymbol{\Pi}_k{}^{-1}\mathrm{vec}\left[\boldsymbol{K}-\hat{\boldsymbol{K}}_k\right]. \quad (11)$$

III. Recognizing Cylindrical Surface

This section provides a method to estimate properties of a cylindrical surface under the situation where the robot's end-effector is in kinetic friction on the surface. An analytical derivation shows that the stiffness matrix under this situation belongs to a certain class. Therefore, a new stiffness matrix has to be found which belongs to this class and which is sufficiently close from $\hat{\boldsymbol{K}}$. Moreover, an uncertainty ellipsoid accompanied by this new estimate must be defined. Normal direction and primary directions are obtained from them.

In this section, the position of the end-effector is substituted by the virtual position $\boldsymbol{p}(t)$, not by the real position $\boldsymbol{p}_{\mathrm{r}}(t)$. The subscripts to denote time index (e.g. k and i) are dropped unless required for clarity.

A. Stiffness Matrix in Sliding on a Cylindrical Surface

Let $\hat{\boldsymbol{p}}$ denote the gravity center of positions that the impedance perception has used to provide $\hat{\boldsymbol{K}}$. Then, $\hat{\boldsymbol{K}}$ can be viewed as the stiffness matrix at position $\hat{\boldsymbol{p}}$. When the end-effector is slid on an object, $\hat{\boldsymbol{p}}$ is usually located below the surface. As shown in Fig.1(a), let $\boldsymbol{p}_U$ denote the projection of $\hat{\boldsymbol{p}}$ onto the surface. And let $\boldsymbol{n}$, $\boldsymbol{t}$, and $\boldsymbol{v}$ be

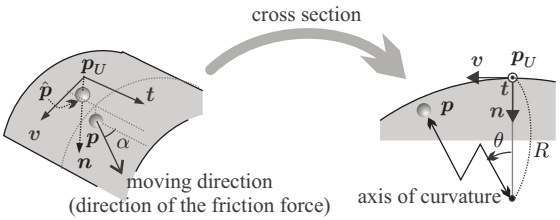

Fig. 1. Sliding on a cylindrical surface

orthonormal vectors which represent the normal direction, the primary direction with the minimum and maximum curvature, at $\hat{\boldsymbol{p}}$, respectively. Let Σ_U be the coordinate system with axes $\{\boldsymbol{n}, \boldsymbol{t}, \boldsymbol{v}\}$ and origin $\boldsymbol{p}_U$. The attitude of Σ_U is expressed by a 3×3 rotation matrix $\boldsymbol{U} \triangleq [\boldsymbol{n}, \boldsymbol{t}, \boldsymbol{v}]$.

Firstly, the force-position relation in the neighborhood of $\hat{\boldsymbol{p}}$ is formulated. Let ${}^U\boldsymbol{p} = [{}^np, {}^tp, {}^vp]^T$ denote the position of the end-effector and ${}^U\boldsymbol{f} = [{}^nf, {}^tf, {}^vf]^T$ denote the force applied to the surface from the end-effector, both relative to Σ_U. The position $\boldsymbol{p}$ and the force $\boldsymbol{f}$, which are relative to the reference coordinate system, are related to ${}^U\boldsymbol{p}$ and ${}^U\boldsymbol{f}$ by $\boldsymbol{p} = \boldsymbol{p}_U + \boldsymbol{U}({}^U\boldsymbol{p})$ and $\boldsymbol{f} = \boldsymbol{U}({}^U\boldsymbol{f}) + \boldsymbol{f}_{\text{weight}}$, where $\boldsymbol{f}_{\text{weight}}$ is the gravitational force on the end-effector and the grasped object. The position $\hat{\boldsymbol{p}}$ relative to Σ_U is written by ${}^U\hat{\boldsymbol{p}} = [{}^n\hat{p}, 0, 0]^T$. As shown in Fig.1, let θ be the angle between the surface normal at $\boldsymbol{p}$ and that at $\boldsymbol{p}_U$, N be the normal force applied to the surface at $\boldsymbol{p}$, R be the curvature radius, and κ be the stiffness of the surface. Then, since $\boldsymbol{p}$ is at the depth of N/κ from the surface, ${}^np$ and ${}^vp$ are written by

$$\begin{bmatrix} {}^np \\ {}^vp \end{bmatrix} = \begin{bmatrix} R(1-\cos\theta) + N/\kappa\cos\theta \\ R\sin\theta - N/\kappa\sin\theta \end{bmatrix}. \tag{12}$$

Let α be the angle between the friction direction and $\boldsymbol{t}$-direction at position $\boldsymbol{p}$ as shown in Fig.1, and let μ be the friction coefficient of the surface. Then, since the friction force magnitude is μN, ${}^U\boldsymbol{f}$ can be written by

$$\begin{bmatrix} {}^nf \\ {}^tf \\ {}^vf \end{bmatrix} = \begin{bmatrix} N\left(\cos\theta + \mu\sin\alpha\sin\theta\right) \\ N\mu\cos\alpha \\ N\left(-\sin\theta + \mu\sin\alpha\cos\theta\right) \end{bmatrix}. \tag{13}$$

Eliminating θ and N from (12) and (13) yields

$$\begin{aligned} {}^nf &= \kappa'\left((R - {}^np) + ({}^vp)\mu\sin\alpha\right) && (14)\\ {}^tf &= \kappa'\mu\cos\alpha\sqrt{(R-{}^np)^2 + ({}^vp)^2} && (15)\\ {}^vf &= \kappa'\left((R-{}^np)\mu\sin\alpha - ({}^vp)\right) && (16)\\ \kappa' &\triangleq \kappa\left(R/\sqrt{(R-{}^np)^2 + ({}^vp)^2} - 1\right). \end{aligned}$$

The stiffness matrix at position $\boldsymbol{p}_U$ is derived as $\boldsymbol{K} = \boldsymbol{U}({}^U\boldsymbol{K}_U)\boldsymbol{U}^T$, ${}^U\boldsymbol{K}_U \triangleq \left(\partial^U\boldsymbol{f}/\partial^U\boldsymbol{p}\right)|_{{}^U\boldsymbol{p}={}^U\hat{\boldsymbol{p}}}$, where ${}^U\boldsymbol{K}_U$ is given by

$${}^U\boldsymbol{K}_U = \begin{bmatrix} \kappa & 0 & \kappa\mu\sin\alpha({}^n\hat{p})/(R-{}^n\hat{p}) \\ \kappa\mu\cos\alpha & 0 & 0 \\ \kappa\mu\sin\alpha & 0 & -\kappa({}^n\hat{p})/(R-{}^n\hat{p}) \end{bmatrix}. \tag{17}$$

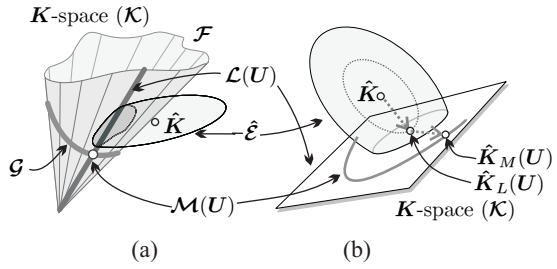

Fig. 2. Inclusive relationship among subsets of $\{\boldsymbol{K} \in \mathcal{R}^{3\times3}\}$

Let the elements of ${}^U\boldsymbol{K}_U = \boldsymbol{U}^T\boldsymbol{K}\boldsymbol{U}$ be denoted by ${}^{nn}\lambda$ ($\triangleq \boldsymbol{n}^T\boldsymbol{K}\boldsymbol{n}$), ${}^{nt}\lambda$ ($\triangleq \boldsymbol{n}^T\boldsymbol{K}\boldsymbol{t}$), and so on. Then, it is shown that, since (17), a stiffness matrix obtained in this situation satisfies the following conditions;

$${}^{nt}\lambda = {}^{tt}\lambda = {}^{vt}\lambda = {}^{tv}\lambda = 0 \tag{18}$$

$$({}^{vn}\lambda)({}^{vv}\lambda) + ({}^{nv}\lambda)({}^{nn}\lambda) = 0. \tag{19}$$

With a given rotation matrix $\boldsymbol{U}$, let $\boldsymbol{\mathcal{L}}(\boldsymbol{U})$ denote the set of $\boldsymbol{K}$'s which satisfy (18), and $\boldsymbol{\mathcal{M}}(\boldsymbol{U})$ denote the subset of $\boldsymbol{\mathcal{L}}(\boldsymbol{U})$ which is defined by (19). Moreover, let $\boldsymbol{\mathcal{F}}$ be the union of all $\boldsymbol{\mathcal{L}}(\boldsymbol{U})$'s, and $\boldsymbol{\mathcal{G}}$ be the union of all $\boldsymbol{\mathcal{M}}(\boldsymbol{U})$'s (Fig.2). Thus it is shown that a stiffness matrix consistent with kinetic friction state on a cylindrical surface is included by $\boldsymbol{\mathcal{G}}$.

B. New Estimate $\hat{\boldsymbol{\mathcal{E}}}_M(\boldsymbol{U})$ with Respect to a Given $\boldsymbol{U}$

Since $\hat{\boldsymbol{K}}$ is generally not included by $\boldsymbol{\mathcal{G}}$, an element of $\boldsymbol{\mathcal{G}}$ which is close from $\hat{\boldsymbol{K}}$ has to be sought. For this purpose, this subsection provides a method to obtain an element of $\boldsymbol{\mathcal{M}}(\boldsymbol{U})$ which is close from $\hat{\boldsymbol{K}}$. In the discussion below, $(\boldsymbol{U})$ is omitted unless required for clarity.

Firstly, the element of $\boldsymbol{\mathcal{L}}$ that minimizes $D(\boldsymbol{K})$, hereinafter $\hat{\boldsymbol{K}}_L$, is derived. Let $\boldsymbol{L} \triangleq \left[\ \boldsymbol{n}\otimes\boldsymbol{U}\ \middle|\ \boldsymbol{v}\otimes[\boldsymbol{n},\boldsymbol{v}]\ \right]$ ($\in \mathcal{R}^{9\times5}$) and $\boldsymbol{\lambda} \triangleq [{}^{nn}\lambda, {}^{tn}\lambda, {}^{vn}\lambda, {}^{nv}\lambda, {}^{vv}\lambda]^T$ ($\in \mathcal{R}^5$). Then, under the condition $\boldsymbol{K} \in \boldsymbol{\mathcal{L}}$, $\mathrm{vec}\,[\boldsymbol{K}] = \boldsymbol{L}\boldsymbol{\lambda}$ holds and $D(\boldsymbol{K})$ can be written by

$$\begin{aligned} D(\boldsymbol{K}) &= (\boldsymbol{\lambda}-\hat{\boldsymbol{\lambda}}_L)^T{\boldsymbol{V}_L}^{-1}(\boldsymbol{\lambda}-\hat{\boldsymbol{\lambda}}_L) + \hat{D}_L && (20)\\ \hat{D}_L &\triangleq \hat{\boldsymbol{k}}^T\boldsymbol{\Pi}^{-1}\hat{\boldsymbol{k}} - {\hat{\boldsymbol{\lambda}}_L}^T\boldsymbol{L}^T\boldsymbol{\Pi}^{-1}\hat{\boldsymbol{k}} && (21)\\ \hat{\boldsymbol{\lambda}}_L &\triangleq \boldsymbol{V}_L\boldsymbol{L}^T\boldsymbol{\Pi}^{-1}\hat{\boldsymbol{k}} && (22)\\ \boldsymbol{V}_L &\triangleq (\boldsymbol{L}^T\boldsymbol{\Pi}^{-1}\boldsymbol{L})^{-1}, && (23) \end{aligned}$$

where $\boldsymbol{\Pi} \triangleq \boldsymbol{P}\otimes\boldsymbol{S}$ and $\hat{\boldsymbol{k}} \triangleq \mathrm{cs}[\hat{\boldsymbol{K}}]$. $\hat{\boldsymbol{\lambda}}_L$ corresponds to $\hat{\boldsymbol{K}}_L$ in the sense that $\mathrm{cs}[\hat{\boldsymbol{K}}_L] = \boldsymbol{L}\hat{\boldsymbol{\lambda}}_L$ (Fig.2(b)), and $\hat{D}_L$ is the generalized distance between $\hat{\boldsymbol{K}}_L$ and $\hat{\boldsymbol{K}}$. Note that $\hat{D}_L$, $\boldsymbol{V}_L$ and $\hat{\boldsymbol{\lambda}}_L$ are functions of $\boldsymbol{U}$. By expressing an element of $\boldsymbol{\mathcal{L}}$ by $\boldsymbol{\lambda}$, the generalized distance from $\hat{\boldsymbol{\lambda}}_L$ to $\boldsymbol{\lambda}$ is defined by $D_L(\boldsymbol{\lambda}) \triangleq (\boldsymbol{\lambda}-\hat{\boldsymbol{\lambda}}_L)^T{\boldsymbol{V}_L}^{-1}(\boldsymbol{\lambda}-\hat{\boldsymbol{\lambda}}_L)$ based on the crosssection hyper-ellipsoid of $\hat{\boldsymbol{\mathcal{E}}}$ with $\boldsymbol{\mathcal{L}}$.

Next, an element of $\boldsymbol{\mathcal{M}}$ that is close from $\hat{\boldsymbol{K}}_L$, denoted $\hat{\boldsymbol{K}}_M$, has to be found. Letting $m(\boldsymbol{\lambda}) \triangleq ({}^{vn}\lambda)({}^{vv}\lambda) +$

$({}^{nv}\lambda)({}^{nn}\lambda)$, this can be written in the form of $m(\boldsymbol{\lambda}) = \boldsymbol{\lambda}^T \boldsymbol{P} \boldsymbol{\lambda}$ where $\boldsymbol{P}$ is a symmetrix 5×5 matrix. In the neighborhood of $\hat{\boldsymbol{\lambda}}_L$, $m(\boldsymbol{\lambda})$ can be linearly approximated by

$$m(\boldsymbol{\lambda}) \approx \tilde{m}(\boldsymbol{\lambda}) \triangleq \boldsymbol{u}^T(\boldsymbol{\lambda} - \hat{\boldsymbol{\lambda}}_L) + \hat{\boldsymbol{\lambda}}_L{}^T \boldsymbol{P} \hat{\boldsymbol{\lambda}}_L \quad (24)$$

$$\boldsymbol{u} \triangleq (\partial m(\boldsymbol{\lambda})/\partial \boldsymbol{\lambda})|_{\boldsymbol{\lambda}=\hat{\boldsymbol{\lambda}}_L} = 2\boldsymbol{P}\hat{\boldsymbol{\lambda}}_L. \quad (25)$$

One can find that under the condition $\tilde{m}(\boldsymbol{\lambda}) = 0$, $\boldsymbol{\lambda}$ which minimizes $D_L(\boldsymbol{\lambda})$ can be expressed by $\boldsymbol{\lambda} = \hat{\boldsymbol{\lambda}}_L + x\boldsymbol{V}_L\boldsymbol{P}\hat{\boldsymbol{\lambda}}_L$ where x is a certain real number. Hence, $\hat{\boldsymbol{\lambda}}_M$ is defined as a $\boldsymbol{\lambda}$ which can be expressed in this form and satisfies $m(\boldsymbol{\lambda}) = 0$. This is found by solving the second order equation $m(\hat{\boldsymbol{\lambda}}_L + x\boldsymbol{V}_L\boldsymbol{P}\hat{\boldsymbol{\lambda}}_L) = 0$ with respect to x. By this means $\hat{\boldsymbol{\lambda}}_M$ and $\mathrm{cs}[\hat{\boldsymbol{K}}_M] \triangleq \boldsymbol{L}\hat{\boldsymbol{\lambda}}_M$ are obtained.

The generalized distance between $\hat{\boldsymbol{K}}$ and $\hat{\boldsymbol{K}}_M$ is $\hat{D}_M \triangleq D(\hat{\boldsymbol{K}}_M) = \hat{D}_L + D_L(\hat{\boldsymbol{\lambda}}_M)$. The uncertainty ellipsoid accompanied by $\hat{\boldsymbol{K}}_M$ can be given by moving $\hat{\boldsymbol{\mathcal{E}}}$ from $\hat{\boldsymbol{K}}$ to $\hat{\boldsymbol{K}}_M$, and magnifying it with respect to $\hat{D}_M$. This ellipsoid, denoted by $\hat{\boldsymbol{\mathcal{E}}}_M$, is defined as follows;

$$\mathrm{vec}\left[\boldsymbol{K} - \hat{\boldsymbol{K}}_M\right] \mathrm{vec}\left[\boldsymbol{K} - \hat{\boldsymbol{K}}_M\right]^T \preceq (1 + \hat{D}_M)\boldsymbol{\Pi} \quad (26)$$

The crosssection of $\hat{\boldsymbol{\mathcal{E}}}_M$ with the hyper plane $\boldsymbol{\mathcal{L}}$ is

$$(\boldsymbol{\lambda} - \hat{\boldsymbol{\lambda}}_M)(\boldsymbol{\lambda} - \hat{\boldsymbol{\lambda}}_M)^T \preceq (1 + \hat{D}_M)\boldsymbol{V}_L. \quad (27)$$

The components of $\hat{\boldsymbol{\lambda}}_M$ and $\boldsymbol{V}_L$ are denoted by ${}^{nn}\hat{\lambda}_M$, ${}^{nn,nn}V_L$, and so on.

C. Feasibility Evaluation of $\hat{\boldsymbol{\mathcal{E}}}_M(\boldsymbol{U})$

Equations (18)(19) gives conditions for feasible $\hat{\boldsymbol{K}}_M(\boldsymbol{U})$, but more conditions are required for $\hat{\boldsymbol{\mathcal{E}}}_M(\boldsymbol{U})$. For example, (17) implies that ${}^{nn}\hat{\lambda}_M(\boldsymbol{U})$ should be positive, and that ${}^{vv}\hat{\lambda}_M(\boldsymbol{U})$ should be negative. Besides, the impedance perception usually provides estimates with small uncertainties in directions in which the position variance is large. This direction is usually the moving direction, and must be consistent with the α-value. However, the analytical (17) and the estimates are consistent only under limited conditions, because (17) are based on the derivatives of the non-linear force-position relation (14)(15)(16), in contrast with the estimates based on sensor observation distributed in a finite volume of space.

Omitting the detailed derivations for space limitations, a consistency criterion is given as follows;

$$\Phi(\boldsymbol{U}) = \beta^2\Phi_{t1}\Phi_{t2}\Phi_{t3} + \Phi_{v1}\Phi_{v2}\Phi_{v3} \quad (28)$$

$$\Phi_{t1}(\boldsymbol{U}) = {}^{tn}\hat{\lambda}_M(\boldsymbol{U})^2 / \left({}^{tn}\hat{\lambda}_M(\boldsymbol{U})^2 + {}^{vn}\hat{\lambda}_M(\boldsymbol{U})^2\right)$$

$$\Phi_{t2}(\boldsymbol{U}) = \left((\boldsymbol{t}\otimes\boldsymbol{t})^T\boldsymbol{\Pi}^{-1}(\boldsymbol{t}\otimes\boldsymbol{t})\right) / (1 + \hat{D}_M(\boldsymbol{U}))$$

$$\Phi_{t3}(\boldsymbol{U}) = \frac{\max\left(0, ({}^{nn}\hat{\lambda}_M(\boldsymbol{U}))\right)^2}{(1 + \hat{D}_M(\boldsymbol{U}))({}^{nn,nn}V_L(\boldsymbol{U}))}$$

$$\Phi_{v1}(\boldsymbol{U}) = {}^{vn}\hat{\lambda}_M(\boldsymbol{U})^2 / \left({}^{tn}\hat{\lambda}_M(\boldsymbol{U})^2 + {}^{vn}\hat{\lambda}_M(\boldsymbol{U})^2\right)$$

$$\Phi_{v2}(\boldsymbol{U}) = \left((\boldsymbol{v}\otimes\boldsymbol{t})^T\boldsymbol{\Pi}^{-1}(\boldsymbol{v}\otimes\boldsymbol{t})\right) / (1 + \hat{D}_M(\boldsymbol{U}))$$

$$\Phi_{v3}(\boldsymbol{U}) = \frac{\min\left(0, ({}^{vv}\hat{\lambda}_M(\boldsymbol{U}))\right)^2}{(1 + \hat{D}_M(\boldsymbol{U}))({}^{vv,vv}V_L(\boldsymbol{U}))}.$$

Here, the ratio between Φ_{t1} and Φ_{v1} is correspondent to the value of α, namely, the moving direction. Φ_{t2} and Φ_{v2} are inverses of the uncertainties of ${}^{tt}\hat{\lambda}_M$ and ${}^{tv}\hat{\lambda}_M$. Φ_{t3} and Φ_{v3} are reliability measures for conditions ${}^{nn}\hat{\lambda}_M > 0$ and ${}^{vv}\hat{\lambda}_M < 0$ respectively. β is a small positive real number for maintaining balance between Φ_{t3} and Φ_{v3} (since $({}^{n}\hat{p}) \ll R$, ${}^{nn}\hat{\lambda}_M$ is usually much larger than ${}^{vv}\hat{\lambda}_M$ as seen in (17)). In the experiments in section IV, $\beta = 0.1$ is used.

By finding $\boldsymbol{U}$ which maximize $\Phi(\boldsymbol{U})$, the estimate of $\boldsymbol{U}$, $\hat{\boldsymbol{U}}$, is obtained. A modified version of the steepest gradient method is employed to obtain $\hat{\boldsymbol{U}} = [\hat{\boldsymbol{n}}, \hat{\boldsymbol{t}}, \hat{\boldsymbol{v}}]$. Consequently, $\hat{\boldsymbol{K}}_G \triangleq \hat{\boldsymbol{K}}_M(\hat{\boldsymbol{U}})$, $\hat{\boldsymbol{\mathcal{E}}}_G \triangleq \hat{\boldsymbol{\mathcal{E}}}_M(\hat{\boldsymbol{U}})$, $\hat{\boldsymbol{\lambda}}_G \triangleq \hat{\boldsymbol{\lambda}}_M(\hat{\boldsymbol{U}})$, $\boldsymbol{V}_F \triangleq \boldsymbol{V}_L(\hat{\boldsymbol{U}})$, and $\hat{D}_G \triangleq \hat{D}_L(\hat{\boldsymbol{U}})$ are obtained.

D. Estimating κ, μ, and R

The stiffness and friction coefficients, κ and μ, and the curvature, $\rho \triangleq 1/R$, of the surface are estimated based on $\hat{\boldsymbol{U}}$, $\boldsymbol{V}_F$ and $\hat{\boldsymbol{K}}_G$.

Firstly, κ can be estiamted as $\hat{\kappa} = {}^{vv}\hat{\lambda}_G$, since (17). This is valid only when the moving direction is almost along $\boldsymbol{v}$ direction, because otherwise (14) becomes highly non-linear with respect to ${}^{n}p$

Based on (17), μ and its uncertainty bound can be estimated as follows;

$$\hat{\mu} = \sqrt{({}^{nt}\hat{\lambda}_G)^2 + ({}^{nv}\hat{\lambda}_G)^2} / |{}^{nn}\hat{\lambda}_G| \quad (29)$$

$$(\mu - \hat{\mu})^2 \leq V_\mu \triangleq \left(\frac{\partial\hat{\mu}}{\partial\hat{\boldsymbol{\lambda}}_G{}^T}\right)^T \boldsymbol{V}_F \left(\frac{\partial\hat{\mu}}{\partial\hat{\boldsymbol{\lambda}}_G{}^T}\right) \quad (30)$$

Finally, again based on (17), ρ can be estimated as $\hat{\rho} = \left(({}^{n}\hat{p}) - \kappa({}^{n}\hat{p})/({}^{vv}\hat{\lambda}_G)\right)^{-1}$. Here, ${}^{n}\hat{p}$ is unknown but letting $\hat{N}$ be the normal force applied to the environment, and considering ${}^{n}\hat{p} = \hat{N}/\kappa$, the following is obtained:

$$\hat{\rho} = \left(\hat{N}/\kappa - \hat{N}/({}^{vv}\hat{\lambda}_G)\right)^{-1}. \quad (31)$$

Here one must note that $\hat{N}$ is the normal force applied to the surface, and can not be derived from the sensor observation at that instant. Due to the non-linearity of (16), (31) holds true only when the variance of ${}^{v}p$ is small, and in this case $\kappa \approx {}^{nn}\hat{\lambda}_G > 0$ may or may not hold. Therefore, when using (31) to estimate the curvature, the stiffness of the surface also must be known. The uncertainty of $\hat{\rho}$ can be defined in the same way as (30).

IV. Experiments

A. Setup and Method

Preliminary experiments were conducted. The setup is as shown in Fig.3(a). It consists of a three-joint miniature

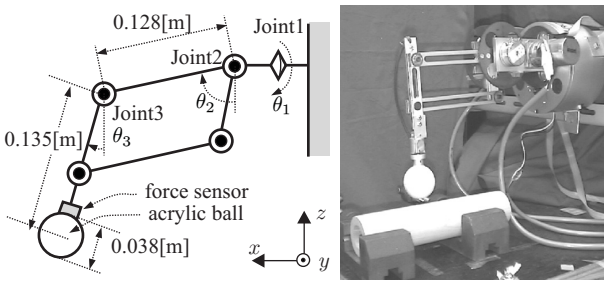

(a) experimental setup

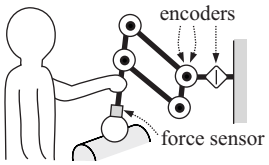

(b) method of experiment

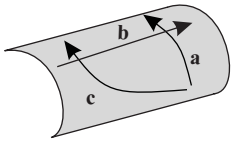

(c) surface following actions

Fig. 3. Experiment

robot arm, a 6-axis force-torque sensor ("NANO Sensor", BL Autotec, LTD.), and an acrylic sphere (diameter 38[mm], a table tennis ball), which is used as the end-effector. The position of the end-effector is measured by the optical encoders attached to the joints. The robot is moved by the experimenter as shown in Fig.3(b) without using the joint actuators.

Two objects, **H** and **S**, were used. Object **H** is a wooden cylinder with diameter of 42[mm]. Object **S** is a soft cylindrical object with diameter 42[mm], which consists of a wooden cylinder with diameter of 24[mm] covered with a soft sponge sheet with thickness of 9[mm]. Three surface following actions, **a**, **b**, and **c**, as shown in Fig.3(c), were performed on each object. These runs are denoted like **Ha**, **Sb**, and so on.

The computer used is with an Intel Pentium III CPU (1[GHz]). The sampling period of the impedance perception is 1.5[msec], and that of the surface property estimation is 15[msec]. $K_{\rm v}$ and $B_{\rm v}$ of the VSF are set to be 700[N/m] and 10[Ns/m] respectively. The weightings of the measurements ($w_{k,i}$ in (6)) are reduced to a half after $1.0{\times}10^{-3}$[m] of distance or 0.1[sec] of time is moved or elapsed. β in (28) is set to be 0.1. Those parameters are designed by trial and error.

The friction coefficients of **H** and **S** are about 0.27 and 0.85, and the stiffness coefficient of **S** is about 320[N/m]. Object **H** can be regarded as rigid. Apparent stiffness coefficients of **H** and **S** estimated through the VSF are expected to be about $K_{\rm v} = 700$[N/m] and $320K_{\rm v}/(K_{\rm v}{+}320) \approx 220$[N/m] respectively. Considering the radius of the end-effector, the estimates of the curvatures are expected to be 2/(43+38[mm])$\approx 25[{\rm m}^{-1}]$ and 2/(42+38[mm])$\approx 25[{\rm m}^{-1}]$ respectively.

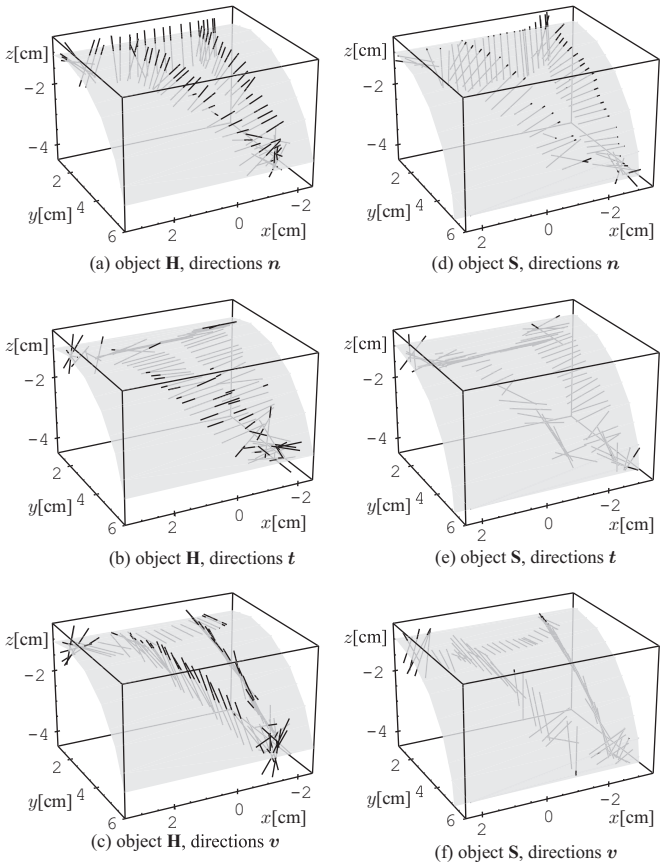

Fig. 4. Estimated directions $\hat{\boldsymbol{n}}$, $\hat{\boldsymbol{t}}$, $\hat{\boldsymbol{v}}$

B. Result

The results are shown in Fig.4 and Fig.5. Fig.4 shows the estimated $\hat{\boldsymbol{n}}$, $\hat{\boldsymbol{t}}$ and $\hat{\boldsymbol{v}}$, and the actual positions of the objects represented by the transparent surfaces. Fig.5 shows the estimated ${}^{nn}\hat{\lambda}_G$, friction coefficient μ, and curvature ρ. Estimated values are represented by black solid curves and their uncertainties are represented by gray bands. The time spans in which the end-effector is in touch with the surfaces are bounded by vertical lines (those represent the discontinuities detected by the impedance perception[7]. Those discontinuities agree with the actual times of contact and separation with the surface. When the discontinuities are detected, the cumulated data of the past, $\boldsymbol{R}_k$, $\boldsymbol{Q}_k$ and $\boldsymbol{F}_k$, are reset to zero). The estimation is performed only when the observed force is larger than a threshold. When the computation does not finish within the sampling period (15[msec]), estimates are not obtained and blanks appear in the graphs.

Fig.4 shows that $\{\boldsymbol{n}, \boldsymbol{t}, \boldsymbol{v}\}$ are properly estimated in most cases. The estimates are stable and correct especially on object **H**, which is non-deformable. Some misestimations follow the collisions, but most of them are limited in the short time periods between the occurrence and detection of the discontinuities. However, on object **S**,

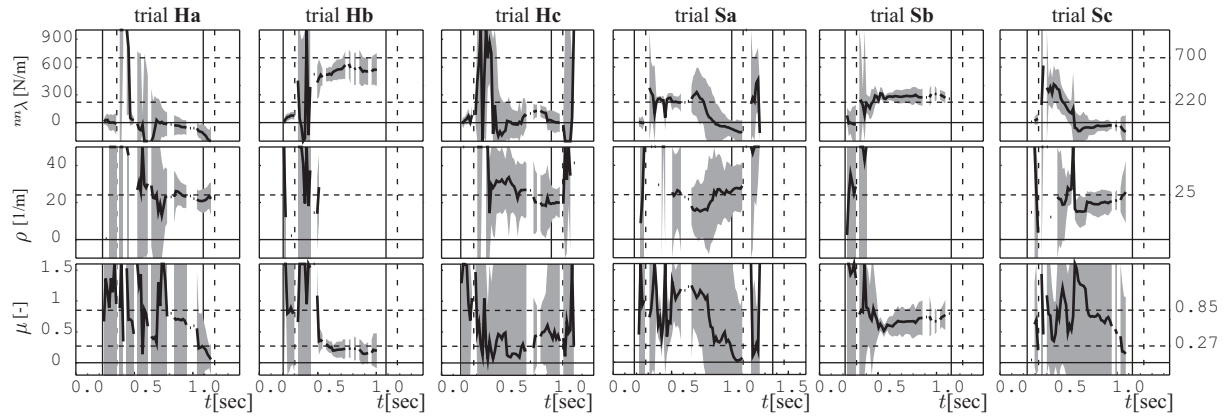

Fig. 5. Estimated stiffness coefficients ${}^{nn}\hat{\lambda}_G$, curvature $\hat{\rho}$, and friction coefficient $\hat{\mu}$

which is deformable, $\boldsymbol{t}$ and $\boldsymbol{v}$ are confused when the motion is not along primary directions, i.e., in action **c**. This may be because the weighting factor β in (28) is not proper. Or more specifically, the criterion $\Phi(\boldsymbol{U})$ may need reconsideration.

${}^{nn}\lambda$ is estimated to be close to the correctly value of κ (700[N/m] for **H** and 220[N/m] for **S**) under action **b**, along the primary direction $\boldsymbol{t}$. The cause of the incorrect estimations in actions **a** and **c** is as explained in III-D.

The friction coefficient μ is correctly estimated (0.27 for **H** and 0.85 for **S**) especially under action **b**. As expected, the uncertainty is large when the estimate is far from the true value. However, sometimes large uncertainties are obtained even when the the estimate is near the true value. The definition of the uncertainty may have to be improved.

Estimation of ρ is performed only when ${}^{vv}\hat{\lambda}_G < 0$. As shown in (31), the stiffness κ and the normal force $\hat{N}$ are required to estimate ρ. $\kappa = 700$[N/m] is used for object **H**, and $\kappa = 220$[N/m] for object **S**. Due to the negligible weight of the end-effector, the observed force is directly used to determine $\hat{N}$. ρ is properly estimated in action **a**, which is along the primary direction $\boldsymbol{v}$, but surface deformability contributes large uncertainty.

V. Conclusion

This paper has proposed a method for extracting information on properties of a convex cylindrical surface, using the stiffness matrix provided by the impedance perception[7], under the situation where the end-effector is slid on the surface. The normal and primary directions can be obtained from the stiffness matrix, and, in limited conditions, the friction and stiffness coefficients also can be obtained. The curvature also can be estimated by using the information on the force applied to the surface. The results of preliminary experiments have been presented. The proposed method still seems to need improvement, but it is shown that this approach can be effective for extracting information on various properties of environment. This method is for passive monitoring of sensor data without requiring any specialized control strategies. Therefore, this has a potential to be used not only for autonomous robots but also for manually controlled robots and, moreover, direct monitoring of human manipulations. The future research should be directed toward enhancing this scheme so that it can deal with general surfaces and more than two constraint hypersurfaces. Quantitative evaluation of the accuracy of the estimation will also be a future topic.

VI. References

[1] A. M. Okamura, M. A. Costa, M. L. Turner, and C. Richard, "Haptic Surface Exploration," in *Experimental Robotics VI*, pp. 423–432. Springer-Verlag, 2000.

[2] M. Skubic and R. A. Volz, "Identifying Single-Ended Contact Formations from Force Sensor Patterns," *IEEE Trans. of Robotics and Automation*, vol. 16, no. 5, pp. 597–602, 2000.

[3] B. J. McCarragher and H. H. Asada, "Qualitative Template Matching Using Dynamic Process Models for State Transition Recognition of Robotic Assembly," *J. of Dynamic Systems, Measurement, and Control*, vol. 115, pp. 261–269, 1993.

[4] P. Dupont, T. M. Schuteis, P. A. Millman, and R. D. Howe, "Automatic Identification of Environment Haptic Properties," *Presence*, vol. 8, no. 4, pp. 394–411, 1999.

[5] M. Charlebois, K. Gupta, and S. Payandeh, "Shape description of curved surfaces using tactile sensing and surface normal information," in *Proc. of the 1997 IEEE Int. Conf. on Robotics and Automation*, 1997, pp. 2819–2824.

[6] M. Moll and M. A. Erdmann, "Dynamic Shape Reconstruction Using Tactile Sensors," in *Proc. of the 2002 IEEE Int. Conf. on Robotics and Automation*, 2002, pp. 1636–1642.

[7] R. Kikuuwe and T. Yoshikawa, "Robot Perception of Environment Impedance," in *Proc. of the 2002 IEEE Int. Conf. on Robotics and Automation*, 2002, pp. 1661–1666.

[8] R. Kikuuwe and T. Yoshikawa, "Recognizing Surface Properties using Impedance Perception," in *Proc. of the 2003 IEEE Int. Conf. on Robotics and Automation*, 2003, (to appear).